THE JOURNAL OF BIOLOGICAL CHEMISTRY

Vol. 266, No. 28, Issue of October 5, pp. 18660-18667, 1991
Printed in U.S.A.

The Molecular Structure of the High Potential Iron-Sulfur Protein Isolated from *Ectothiorhodospira halophila* Determined at 2.5-Å Resolution*

(Received for publication, May 16, 1991)

Deborah R. Breiter‡, Terrance E. Meyer§, Ivan Rayment¶, and Hazel M. Holden‡‖

From the Departments of ‡Chemistry and the Institute for Enzyme Research, University of Wisconsin, Madison, Wisconsin 53705, the §Department of Biochemistry, University of Arizona, Tucson, Arizona 85721, and the ¶Department of Biochemistry and the Institute for Enzyme Research, University of Wisconsin, Madison, Wisconsin 53705

The molecular structure of a high potential iron-sulfur protein (HiPIP) isolated from the purple photosynthetic bacterium, *Ectothiorhodospira halophila* strain BN9626, has been solved by x-ray diffraction analysis to a nominal resolution of 2.5 Å and refined to a crystallographic *R* value of 18.4% including all measured x-ray data from 30.0- to 2.5-Å resolution. Crystals used in the investigation contained two molecules/asymmetric unit and belonged to the space group $P2_1$ with unit cell dimensions of $a = 60.00$ Å, $b = 31.94$ Å, $c = 40.27$ Å, and $\beta = 100.5°$. An interpretable electron density map, obtained by combining x-ray data from one isomorphous heavy atom derivative with non-crystallographic symmetry averaging and solvent flattening, clearly showed that this high potential iron-sulfur protein contains 71 amino acid residues, rather than 70 as originally reported. As in other bacterial ferredoxins, the [4Fe-4S] cluster adopts a cubane-like conformation and is ligated to the protein via four cysteinyl sulfur ligands. The overall secondary structure of the *E. halophila* HiPIP is characterized by a series of Type I and Type II turns allowing the polypeptide chain to wrap around the [4Fe-4S] prosthetic group. The hydrogen bonding pattern around the cluster is nearly identical to that originally observed in the 85-amino acid residue *Chromatium vinosum* HiPIP and consequently, the 240 mV difference in redox potentials between these two proteins cannot be simply attributed to hydrogen bonding patterns alone.

The high potential iron-sulfur proteins, referred to by the acronym HiPIPs, are a class of [4Fe-4S] ferredoxins commonly found in the purple phototrophic bacteria (Bartsch, 1978). These proteins undergo a reversible one-electron transfer reaction at a characteristically high oxidation-reduction midpoint potential of between +50 to +450 mV and are paramagnetic in the oxidized state (Meyer *et al.*, 1983). As a class of ferredoxins, the HiPIPs show significant variation in their amino acid sequences, in their sizes, and in their oxidation-reduction potentials (Tedro *et al.*, 1985; Meyer *et al.*, 1983). The [4Fe-4S] prosthetic groups observed in the HiPIPs are widely distributed in nature and are found, for example, in the low potential bacterial ferredoxins as well as in such enzymes as hydrogenase, nitrogenase, trimethylamine dehydrogenase, and sulfite reductase (Spiro, 1982). Oxidation-reduction potentials associated with these [4Fe-4S] clusters vary enormously, anywhere from −400 mV for the 8Fe ferredoxin from *Peptococcus aerogenes* to +350 mV for the *Chromatium vinosum* HiPIP (Thomson, 1985). Consequently, while the actual biological role of the HiPIPs in anaerobic electron transport is unclear, these proteins provide important models for understanding the structural features that control redox properties of the iron-sulfur cluster.

The three-dimensional structure of one HiPIP, isolated from *C. vinosum*, has been solved by x-ray crystallographic techniques and refined to a nominal resolution of 2.0 Å (Carter *et al.*, 1974; Freer *et al.*, 1975). The overall molecular fold of this protein consists of a three-stranded twisted anti-parallel β-pleated sheet at the carboxyl terminus and two short helical segments at the amino-terminal end of the molecule with the iron-sulfur cluster adopting a cubane-like conformation.

Perhaps one of the most interesting concepts to emerge from the high resolution structural analysis of the *C. vinosum* HiPIP was the formulation of the "three-state hypothesis" which proposed that three oxidation states are available to the [4Fe-4S] cluster with formal charges of −1, −2, and −3 (Carter *et al.*, 1972). This theory was invoked to account for the very different oxidation-reduction potentials and EPR spectra of the bacterial ferredoxins which also contain [4Fe-4S] clusters but have redox potentials of near −400 mV (Strombaugh *et al.*, 1976). Accordingly, the HiPIPs transfer electrons between the first two states whereas the low potential ferredoxins utilize the latter pair of oxidation states. Factors thought to be responsible for the variation of the redox potentials include the exposure of the [4Fe-4S] cluster to the solvent, the presence of aromatic residues near the prosthetic group, the flexibility of the polypeptide chain, and the hydrogen bonding pattern to the redox center. It has been proposed that there is a correlation between redox potentials and the number of backbone N–H hydrogen bonds to sulfur atoms in the cluster (Carter, 1977).

Within recent years enormous effort has been directed toward understanding those factors involved in the modulation of the oxidation-reduction potentials of various redox proteins including the HiPIPs. While it is apparent that the surrounding protein environment determines which oxidation states are available to the iron-sulfur cluster, the exact nature of how this occurs in molecular terms is still not well defined. In an effort to provide a more detailed structural basis for understanding the functional differences between the various [4Fe-4S] ferredoxins, we have been studying, by x-ray crys-

* This research was supported in part by Grant GM39082 from the National Institutes of Health (to H. M. H.) and National Science Foundation Grant DMB-8718678 (to T. E. M.). The costs of publication of this article were defrayed in part by the payment of page charges. This article must therefore be hereby marked "*advertisement*" in accordance with 18 U.S.C. Section 1734 solely to indicate this fact.

‖ To whom correspondence should be addressed.

TABLE I

Intensity statistics for the native and derviative crystals

	Resolution range														
	∞ to 9.64	6.83	5.58	4.84	4.33	3.95	3.66	3.42	3.23	3.06	2.92	2.79	2.69	2.59	2.50
Native															
Average intensity	1968	1615	1829	2157	1865	2331	2079	1570	1326	1047	753	607	562	476	442
Average sigma	414.6	147.8	169.2	173.8	164.5	209.1	154.3	103.7	110.1	95.1	99.8	78.8	81.1	80.8	76.1
R factor[a,b]	0.099	0.055	0.049	0.048	0.049	0.051	0.044	0.044	0.055	0.059	0.080	0.088	0.095	0.115	0.124
$(CH_3)_3PbOOCCH_3$															
Average intensity	1852	1881	2263	2339	2051	2493	2277	1698	1473	1188	859	748	649	576	524
Average sigma	191.6	68.5	93.5	82.9	88.7	81.2	98.8	63.8	67.1	55.9	35.9	37.8	38.1	34.4	37.7
R factor[a,b]	0.029	0.016	0.018	0.018	0.019	0.016	0.017	0.019	0.025	0.025	0.025	0.030	0.034	0.039	0.044

[a] R factor = $\Sigma | I - \bar{I} | / \Sigma I$.
[b] For these statistics, the Friedel pairs were not merged.

TABLE II

Refined heavy atom parameters

x, y, and z are the fractional atomic coordinates, and β is the thermal factor in A^2 and was not refined.

Derivative	Site no.	Relative occupancy	x	y	z	β	Location
$(CH_3)_3PbOOCCH_3$	1	0.9662	0.6400	0.0000	0.9378	15.0	Near the carbonyl oxygen of Asp-18; Molecule II
	2	2.0372	0.9700	0.8625	0.8311	15.0	Glu-32; Molecule II
	3	0.7117	0.7478	0.8909	0.2871	15.0	Asp 11; Molecule I
	4	0.7583	0.8674	0.7218	0.0263	15.0	Glu-15; Molecule II
	5	1.1901	0.7539	0.6491	0.8457	15.0	Glu-27; Molecule II

TABLE III

Phase calculation statistics

	Resolution range							
	∞ to 8.86	5.64	4.42	3.76	3.32	3.01	2.77	2.58
No. of reflections	272	438	566	654	728	802	876	904
Figure of merit	0.40	0.30	0.39	0.38	0.37	0.33	0.30	0.31
Phasing power $((CH_3)_3PbOOCCH_3)$								
Acentric reflections	1.31	1.31	1.35	1.31	1.42	1.44	1.44	1.46
Centric reflections	0.89	0.75	0.96	0.87	0.95	0.78	0.81	1.09

TABLE IV

Refinement statistics

Resolution limits (Å)	30.0–2.5
Initial *R* factor (%)[a]	37.2
Final *R* factor (%)	18.4
No. of cycles of refinement and model building	22
No. of reflections used	5,333
No. of atoms	1,119
No. of solvent molecules	105
Weighted root-mean-square deviations from ideality	
Bond length (Å)	0.014
Bond angle (degree)	2.221
Planarity (trigonal) (Å)	0.003
Planarity (other planes) (Å)	0.007
Torsion angle (degree)[b]	19.437

[a] R factor = $\Sigma | F_o - F_c | / \Sigma | F_o |$.
[b] The torsion angles were not restrained during the refinement.

tallography, the structures of a variety of HiPIPs (Holden *et al.*, 1986a, 1986b). The main advantage of using the HiPIPs to explore structure-function relationships is that they are generally small proteins displaying a wide range of redox potentials, amino acid sequences, and sizes, and when crystals are obtained they generally diffract to very high resolution.

One of the HiPIPs under investigation in our laboratory is isolated from the extremely halophilic purple bacterium *Ectothiorhodospira halophila*. Unlike most purple bacteria, this bacterium produces two HiPIP isozymes referred to as iso-I and iso-II (Tedro *et al.*, 1985). These proteins are the most acidic of the HiPIPs so far isolated with net charges of −11 and −14, respectively (Meyer *et al.*, 1983). Moreover, they have the lowest redox potentials yet reported for proteins in this class with midpoint potentials of +120 and +50 mV, respectively (Meyer *et al.*, 1983). In this report, we describe the three-dimensional structure determination of the *E. halophila* strain BN 9626 iso-I HiPIP to 2.5-Å resolution and compare its structure to that of the *C. vinosum* molecule.

MATERIALS AND METHODS

Crystallization and Preparation of a Heavy Atom Derivative—The *E. halophila* HiPIP isozymes were isolated and purified as described elsewhere (Meyer, 1985). Crystals of iso-I were grown as previously reported with one modification (Holden *et al.*, 1986b). In order to ensure a reproducible supply of large x-ray quality crystals, the technique of macro-seeding was employed (Thaller *et al.*, 1981, 1985; Holden *et al.*, 1988). For such experiments, small HiPIP crystals previously grown from 3.7 M ammonium sulfate solutions buffered with 50 mM Na^+/K^+ phosphate, pH 7.5, were washed with 3.2 M ammonium sulfate solutions again buffered with 50 mM Na^+/K^+ phosphate and containing 5 mM sodium azide. These small seeds were then transferred to droplets (composed of 10 μl of protein and 10 μl of 3.2 M ammonium sulfate, 50 mM Na^+/K^+ phosphate, 5 mM sodium azide) that had been equilibrated by vapor diffusion against 3.2 M ammonium sulfate, 50 mM Na^+/K^+ phosphate, 5 mM sodium azide for 4 days. The resulting "seeded" droplets were subsequently equilibrated at room temperature against 3.5 M ammonium sulfate using the hanging drop method of vapor diffusion. Crystal growth

was normally complete within 6 weeks with the crystals achieving typical dimensions of 1.5 × 0.25 × 0.15 mm. The crystals belong to the space group $P2_1$ with unit cell dimensions of a = 60.00 Å, b = 31.94 Å, c = 40.27 Å, β = 100.5° and two molecules/asymmetric unit as previously reported (Holden *et al.*, 1986b).

For heavy atom derivative searches, native crystals were transferred to 3.8 M ammonium sulfate solutions buffered with 50 mM Na^+/K^+ phosphate, pH 7.5, and containing various heavy atom compounds. The binding of heavy atoms to the crystalline protein was monitored by precession photography. Only one useful heavy atom derivative was prepared by soaking the crystals in 20 mM trimethyllead acetate for 14 days.

X-ray Data Collection and Processing—Three-dimensional x-ray data sets to 2.5-Å resolution from the native and lead-containing crystals were collected at 4 °C using the Siemens area detector system and the data processing package BUDDHA (Blum *et al.*, 1987). Only one crystal was required per x-ray data set. The x-ray source was nickel-filtered copper $K\alpha$ radiation from a Rigaku RU200 x-ray generator operated at 50 kV and 50 mA. Relevant data collection statistics may be found in Table I. The derivative data set was scaled to the native x-ray data in shells of equal volume in reciprocal space based on resolution. Each shell contained approximately 250 reflections. The overall R factor between the native and the derivative x-ray data set was 22.0%, where $R = \Sigma | |F_N| - |F_H| | / \Sigma |F_N|$; $|F_N|$ is the native structure factor amplitude and $|F_H|$ is the derivative structure factor amplitude. Both the native and derivative x-ray data sets contain close to 100% of the total theoretical number of observations to 2.5-Å resolution.

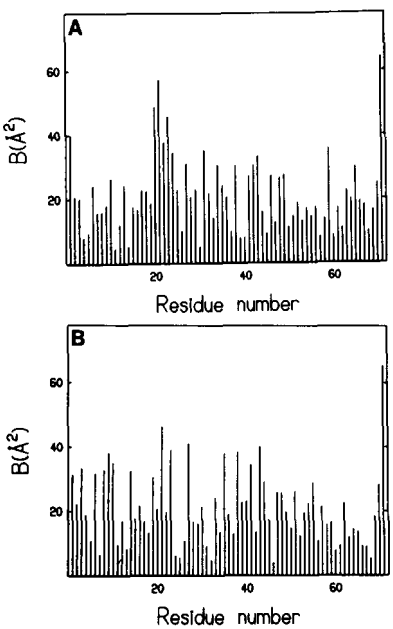

FIG. 1. **Plot of the mean main chain B values *versus* amino acid residue.** Shown are the mean main chain temperature factors for Molecule I in the asymmetric unit (A) and the mean main chain temperature factors for Molecule II in the asymmetric unit (B). The average temperature factor for all backbone atoms was 20.6 Å² for Molecule I and 20.8 Å² for Molecule II.

Computational Methods—The positions of the lead-binding sites within the crystalline lattice were determined by inspection of a difference Patterson map calculated with x-ray data from 30.0- to 3.0-Å resolution. Positions, occupancies, and thermal parameters for the heavy atoms were refined with the origin-removed Patterson-function correlation method (Rossmann, 1960; Terwilliger and Eisenberg, 1983) and these refined parameters may be found in Table II.

Protein phases based on the lead derivative were calculated with the program HEAVY (Terwilliger and Eisenberg, 1983) and relevant phase calculation statistics are given in Table III. The phasing did not include anomalous scattering information from the lead derivative. Also, the anomalous scattering arising from the iron-sulfur clusters was not used in the phasing for two reasons. First, the crystals were very thin plates which introduced an absorption error into the x-ray data that was larger than the anomalous signal itself. This absorption error was, unfortunately, not removed by the data reduction software for area detector images. Second, use of the anomalous signal would have required positioning both [4Fe-4S] clusters within the unit cell from a native anomalous Patterson function. Although it would have been fairly easy to locate the overall positions of these clusters within the unit cell, deriving the exact orientation of the clusters from the anomalous Patterson function would have been a much more difficult task.

An electron density map, phased with the single heavy atom derivative, was calculated with x-ray data from 30.0- to 3.0-Å resolution. Although the map was noisy the positions of the two [4Fe-4S] clusters within the asymmetric unit were immediately obvious as the highest peaks with cube-like structures. Since there were two independent molecules in the asymmetric unit it was possible to improve the quality of the protein phases by the techniques of molecular averaging and solvent flattening. The necessary rotational and translational matrices relating the two molecules within the asymmetric unit for molecular averaging were determined and refined by the program MUNCHKINS (developed in this laboratory by G. Wesenberg and I. Rayment and described in Rypniewski *et al.*, 1991). An averaged electron density map based on these matrices was calculated, plotted onto transparencies, and stacked on Plexiglas sheets. Visual examination of this electron density map clearly revealed the protein-solvent boundaries for the "averaged" HiPIP. A molecular envelope was subsequently drawn around the molecule, digitized on a Calcomp digitizing board and converted into a logical mask by a series of computer programs written by I. Rayment and G. Wesenberg. These programs are available upon request. This molecular mask was used for the subsequent refinement of the protein phases by iterative molecular averaging and solvent flattening (Bricogne, 1976). The initial averaging was performed at 3.0-Å resolution for 15 cycles; the initial protein phases, based on the single isomorphous derivative, were discarded after the first cycle. The structure factor weighting algorithm used in the averaging process was of the form $w = e(||F_o| - |F_c||)/|F_o|$, where $|F_o|$ was the observed structure factor amplitude and $|F_c|$ was the calculated structure factor amplitude (Rayment, 1983). This weighting function governs the contribution of a reflection to the next electron density map calculation and enhances the rate of convergence of the phase refinement. The resolution was extended to 2.5 Å in 0.1 Å increments by including the single isomorphous heavy atom derivative phases for each new wedge of x-ray data for the first cycle, followed by 15 cycles of refinement at the corresponding resolution. The final R factor between the calculated struc-

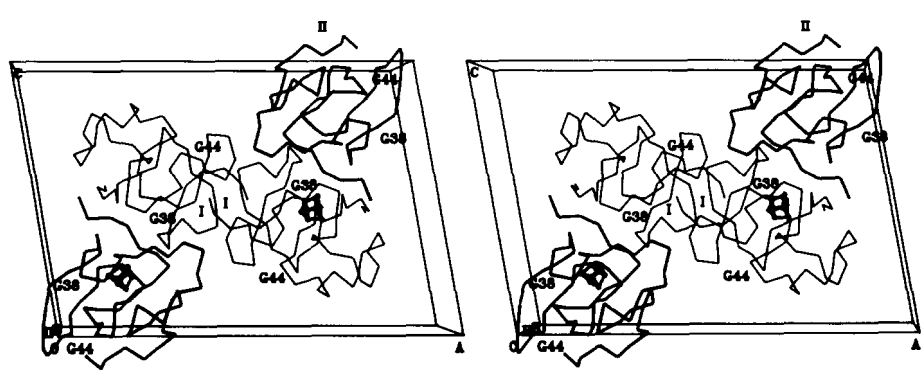

FIG. 2. **Packing diagram of the *E. halophila* unit cell.** The packing of the four molecules in the $P2_1$ unit cell is shown in stereo. The two molecules that constitute the asymmetric unit are shown with their [4Fe-4S] prosthetic groups. Molecule I and its symmetry-related partner are drawn in *thin lines* whereas Molecule II and its symmetry related partner are displayed in *bold lines*. The loops delineated by amino acid residues Gly-38 to Gly-44 adopt slightly different conformations in the two molecules in the asymmetric unit.

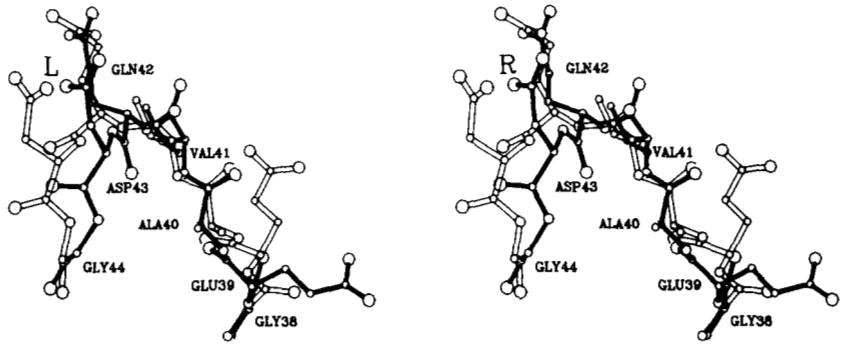

FIG. 3. **Superposition of the loops formed by amino acid residues Gly-38 to Gly-44.** As can be seen from the stereo drawing, the two molecules in the asymmetric unit differ in this loop region as a result of crystal packing. Molecule I is shown in *bold lines* while Molecule II is shown in *open bonds*.

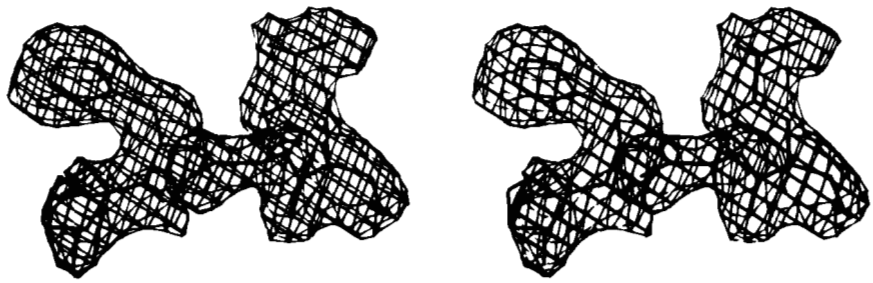

FIG. 4. **Electron density corresponding to amino acid residues 19–23.** The original amino acid sequence determined by Tedro *et al.* (1985) for this region of the HiPIP molecule was Pro-19, Ser-20, His-21, and Gly-22. As can be seen from the above stereo drawing of the electron density map calculated to a nominal resolution of 2.5 Å with coefficients of the form $(2F_o - F_c)$, there is enough density to accommodate another amino acid between Ser-20 and His-21. Furthermore, the electron density for the side chain of Pro-19 was very weak, and the electron density for the side chain of Gly-23 was unusually bulky. After re-evaluation of the amino acid sequence data, the correct sequence is now believed to be Ala-19, Ser-20, Gly-21, His-22, and Pro-23 as built into the above electron density map.

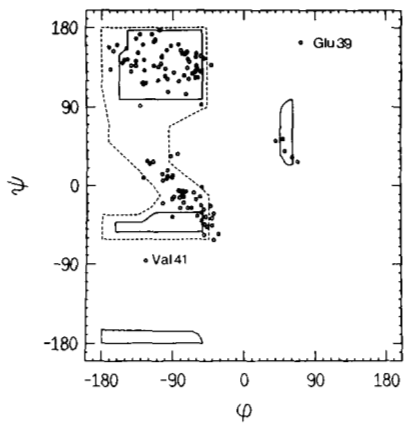

FIG. 5. **Ramachandran plot of all non-glycinyl main chain dihedral angles for the two HiPIP molecules in the asymmetric unit.** Fully allowed ϕ, ψ, values are enclosed by *solid lines*; those only partially allowed are enclosed by *dashed lines*. The 2 amino acid residues that lie outside the allowed regions (Glu-39 and Val-41) belong to Molecule I. They are located in the *loop region* that experiences different molecular packing in the two independent molecules in the asymmetric unit. At the resolution of this investigation, however, it is not apparent why these amino acid residues adopt backbone conformations that are outside the allowed regions.

ture factors from the averaged electron density map and the observed x-ray data was 17.9%. The resulting electron density map confirmed the choice of hand of the heavy atom constellation in that the α-helical turn was right-handed.

A model of the polypeptide chain, based on the primary structure determined by Tedro *et al.*, 1985, was built into the averaged electron density map with the molecular modeling program FRODO (Jones, 1985) and the Evans and Sutherland PS390 graphics system. Twenty-two cycles of alternate least squares refinement with the package TNT (Tronrud *et al.*, 1987) and model building reduced the R factor from 39.2 to 18.4%. The positions and the temperature factors for the individual protein atoms and 105 solvent molecules were refined. The occupancies of the solvent molecules were set to unity. "Ideal" stereochemistry for the [4Fe-4S] cluster was based on the small molecule structure determination of $Fe_4(NO)_4(\mu_3\text{-}S)_4$ by Chu *et al.*, 1982. Relevant refinement statistics may be found in Table IV and the distribution of the mean main chain temperature factors are given in Fig. 1.

RESULTS AND DISCUSSION

The initial model for the iso-I HiPIP from *E. halophila* was built into an averaged and solvent flattened electron density map with the aid of the amino acid sequence determined by Tedro *et al.*, 1985. Although most of the electron density was well-ordered, there were two regions delineated by amino acid residues 19–22 and 38–44 that presented difficulties in the fitting process. The initial problems in fitting amino acid residues 38–44 were strictly due to the averaging process. These residues adopt quite different conformations due to crystal packing as shown in Figs. 2 and 3. The difficulties with residues 19–21 were due to errors in the amino acid sequence. The reported sequence for residues 19–22 is Pro-Ser-His-Gly (Tedro *et al.*, 1985). After several cycles of least squares refinement in which the two independent molecules in the asymmetric unit were no longer constrained to be structurally equivalent, it became obvious that there was another small amino acid residue inserted between Ser-20 and His-21, that residue 22 was a proline rather than a glycine and that residue 19 appeared more like an alanine residue instead of a proline. At the time the original amino acid sequence was determined by Tedro *et al.*, 1985, the amino acid composition of the whole protein and of the three peptides from this region contained between 0.3 and 0.5 more alanine than was expected. Furthermore, the amino acid sequence in this region of question was based on results from a single low-yielding peptide. After re-evaluating the original

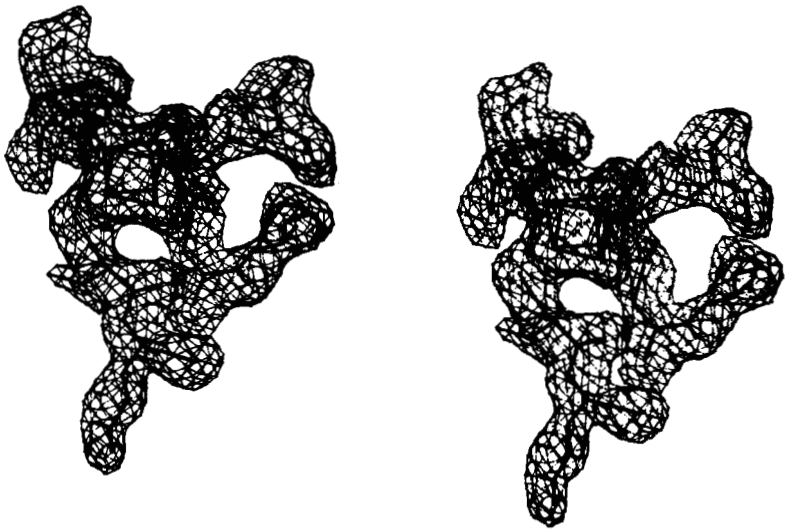

FIG. 6. **Electron density corresponding to the [4Fe-4S] prosthetic group.** The electron density shown was calculated to a nominal resolution of 2.5 Å with coefficients of the form $(2F_o - F_c)$ and corresponds to the area immediately surrounding the iron-sulfur cluster. The protein model was built by using an Evans and Sutherland PS390 graphics system and the molecular modeling program FRODO (Jones, 1985).

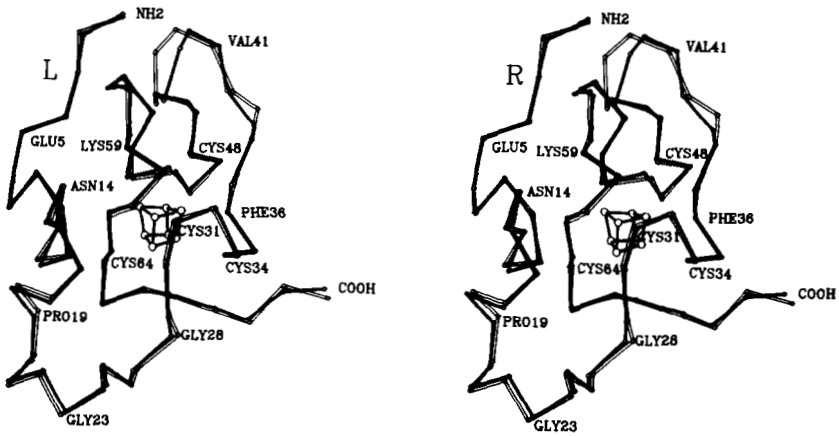

FIG. 7. **Superposition of the α-carbons of the two independent molecules in the asymmetric unit.** The two molecules in the asymmetric unit were superimposed according to the algorithm of Rossmann and Argos (1975). Molecule I is shown in *solid lines* while Molecule II is drawn in *open bonds*. Amino acid residues are labeled at various positions to aid the reader in following the course of the polypeptide chain. This figure was generated with the plotting software package PLUTO, originally written by Dr. Sam Motherwell and modified for proteins by Drs. Eleanor Dodson and Phil Evans.

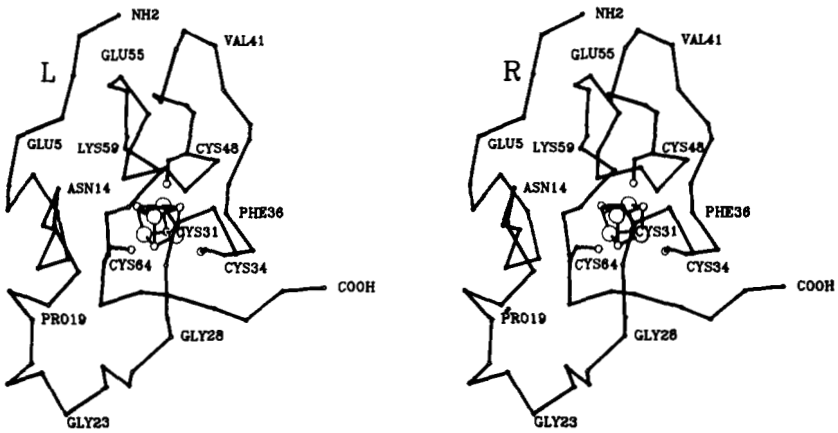

FIG. 8. **Stereoview of the α-carbon model of Molecule I.** For simplicity only the positions of the α-carbons are represented. The iron-sulfur cluster is shown as an atomic model.

amino acid sequence data and in consideration of the present electron density maps, the amino acid sequence is now believed to be Ala-Ser-Gly-His-Pro. Consequently, the iso-I HiPIP contains 71 rather than 70 amino acid residues as originally reported. The electron density corresponding to this region is shown in Fig. 4.

The two HiPIP molecules in the asymmetric unit have now been refined to a nominal resolution of 2.5 Å with a crystallographic *R* factor of 18.4% including all measured x-ray data and maintaining good stereochemical geometry. A plot of the main-chain dihedral angles for both molecules in the asymmetric unit is shown in Fig. 5 and a representative portion of the electron density map near the iron-sulfur cluster is shown in Fig. 6. The quality of the electron density shown in Fig. 6 is consistent throughout the map with the only exceptions being side chains 24 and 43 in both molecules in the asymmetric unit that appear somewhat disordered at this stage of the structural analysis.

The superposition of both molecules in the asymmetric unit is shown in Fig. 7. The α-carbon positions of these two molecules superimpose with a root-mean-square value of 0.67 Å. If amino acid residues 38–44 and 70–71 are removed from the calculation, then the two molecules superimpose with a root-mean-square value of 0.29 Å. For the sake of clarity, the following discussion of the HiPIP structure will only consider one of the molecules in the asymmetric unit, namely the molecule notated as *I* in Fig. 2.

As can be seen in Fig. 8, there are few classical secondary

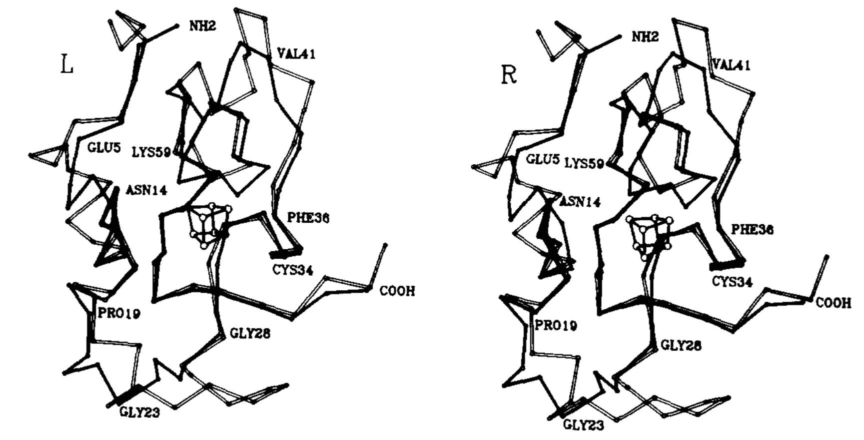

FIG. 9. **Superposition of the structures of the *C. vinosum* and the *E. halophila* HiPIPs.** The structure of the *C. vinosum* HiPIP is shown as *open bonds* whereas the model for the *E. halophila* protein is displayed as *solid lines.* X-ray coordinates for the *C. vinosum* HiPIP were obtained from the Brookhaven Protein Data Bank. The amino acids that are labeled correspond to those found in the *E. halophila* molecule.

```
                                  10        20        30        40        50        60        70        80
Chromatium             SAPANAVAANDATAIALKYNQDATKSERVAAARPGLPPEEQHCANCQFMQADAAGATDEWKGCQLFPGKL-INV--DGWCASWTLKAG
vinosum

                                       10        20        30        40        50        60        70
Ectothiorhodospira          EPRAEDGHAHDYVNEAADP---SHGR-YQEGQ--LCENCAFWGEAVQ---DGWGRCT-HPDFDEVLVKAEGWCSVYAPAS
halophila Iso-I (a)

                            3       11     18           27        38    45  48   57           70
Ectothiorhodospira          RA       DYVNEAAD            EGQLCENCAFWG    WGRC    L-VKA--EGWCSVYAPA
halophila Iso-I (b)
```

FIG. 10. **Amino acid sequence alignments of the *C. vinosum* and the *E. halophila* HiPIPs.** The amino acid sequence for the *C. vinosum* molecule shown here was determined by Dus *et al.*, 1971. Below the *C. vinosum* sequence is the original alignment of the *E. halophila* amino acid sequence determined by Tedro *et al.*, 1985 (*a*) and the new alignment based on three-dimensional similarities (*b*). For the alignment shown in *b* only those amino acids that are structurally similar between the two HiPIPs are given.

structural elements in the *E. halophila* HiPIP. The polypeptide chain basically wraps around the [4Fe-4S] cluster in a random-coil configuration that is punctuated by tight turns. Specifically, there is one α-helical turn (amino acid residues 16–18), three approximate Type II turns (amino acid residues 5–8, 26–29, and 42–45), and six approximate Type I turns (amino acid residues 19–22, 22–25, 30–33, 34–37, 50–53 and 59–62). There is also a very short stretch of anti-parallel β-pleated sheet comprised of amino acid residues 12–13 and 63–64. The [4Fe-4S] cluster is covalently attached to the protein via cysteine residues 31, 34, 48, and 64.

A comparison of the α-carbon traces for the HiPIPs isolated from *E. halophila* and *C. vinosum* is shown in Fig. 9. The *C. vinosum* molecule contains 85 amino acid residues. X-ray coordinates for the *C. vinosum* HiPIP were determined by Carter *et al.* (1974) and were obtained from the Brookhaven Protein Data Bank (Bernstein *et al.*, 1977). The α-carbons of these two molecules superimpose with a root-mean-square value of 0.43 Å for 38 structurally equivalent amino acid residues according to the algorithm of Rossmann and Argos (1972). As expected, the two molecules have similar three-dimensional structures particularly around the immediate vicinity of the iron-sulfur cluster. An amino acid sequence alignment of these HiPIPs based on the tertiary homology is given in Fig. 10 and is quite different from the original alignment based on primary structure alone (Tedro *et al.*, 1985). There are 13 amino acid residues that are both identical and structurally equivalent in these two proteins.

The insertions and deletions between the *E. halophila* and the *C. vinosum* HiPIPs are not neatly placed at the ends of surface loops as frequently observed in other proteins. Instead, there are local rearrangements of structure near the points of insertions such that it is still not possible to determine exactly how many insertions there are nor where they should be placed. It appears that a minimum of four internal insertions and deletions separate the *C. vinosum* and *E. halophila* HiPIPs. The first 4-residue insertion is somewhere between amino acid residues 6–10, the second 5-residue insertion is somewhere between amino acid residues 19–26, the third 3-residue insertion lies between amino acid residues 38–44, and the fourth 2-residue deletion appears to be at amino acid residues 50 and 51. There are 8 other amino acid residues in the *E. halophila* molecule (amino acid residues 5, 6, 19, 49, and 53–56) that are structurally displaced from the *C. vinosum* HiPIP by a small amount due to these insertions and deletions, but they should be considered nearly equivalent.

Those amino acid residues that are approximately 4.0 Å from the iron-sulfur clusters in the *E. halophila* and the *C. vinosum* HiPIPs are shown in Fig. 11, *A* and *B*, respectively. It has been suggested that Tyr-19 in the *C. vinosum* protein plays a critical role in modulating the physicochemical properties of the chromophore (Carter *et al.*, 1974, 1977; Sheridan *et al.*, 1981). As can be seen, Tyr-19 in the *C. vinosum* molecule is indeed spatially conserved in the *E. halophila* molecule as Tyr-12. Other amino acid residues strictly conserved in the binding pocket between these two proteins include Trp-63, Phe-36, and Phe-53 (*E. halophila* numbering). There are 6 aromatic residues surrounding the cluster in the *E. halophila* protein and 5 such residues near the *C. vinosum* cluster. Tyr-67 and Trp-37 in the *E. halophila* HiPIP are replaced by Trp-80 and Met-49, respectively, in the *C. vinosum* protein. Note that while Phe-53 and Phe-66 in the *E. halophila* and the *C. vinosum* proteins, respectively, are conserved, their side chains adopt quite different conformations as can be seen in Fig. 11, *A* and *B*.

The oxidation-reduction potential for the *C. vinosum* HiPIP is +360 mV whereas for the *E. halophila* HiPIP iso-I it is only +120 mV (Meyer *et al.*, 1983). It is possible that the difference in side chain conformation of the above-mentioned phenylalanines may be one of many subtle factors involved in the modulation of oxidation-reduction potentials. Also, the binding pocket for the [4Fe-4S] cluster is somewhat more hydrophobic in the *E. halophila* protein with Ser to Val-66, Thr to Ala-68, and Leu to Thr-49 plus His-50 substitutions. The more hydrophobic environment would favor the oxidized form of the cluster with its lower formal charge of −1 and

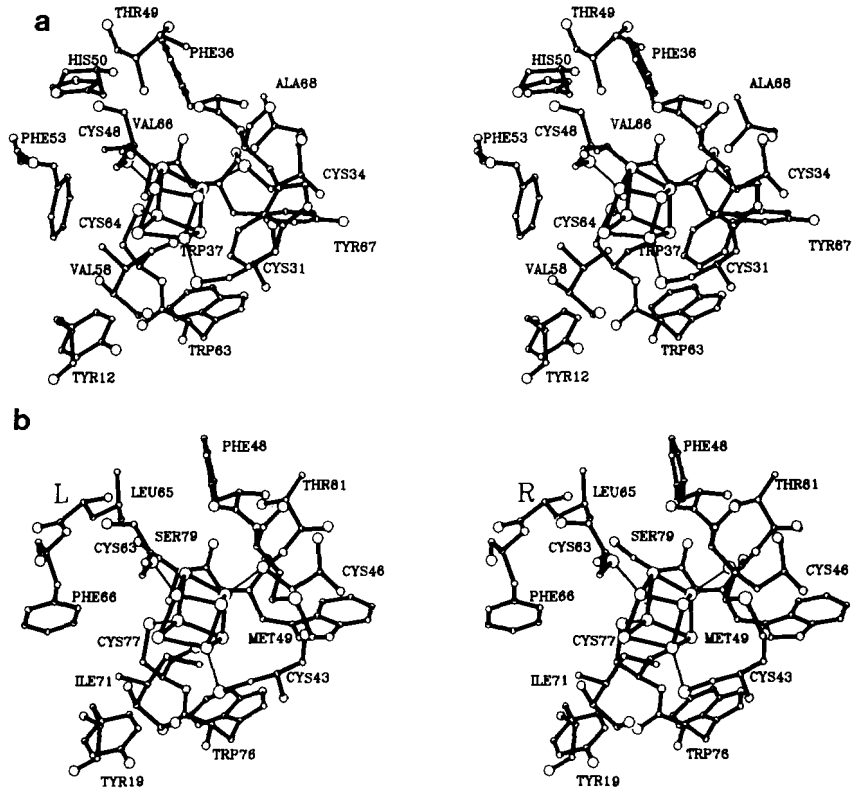

FIG. 11. **Close-up view of the iron-sulfur cluster binding sites for the *E. halophila* and *C. vinosum* HiPIPs.** Only those amino acid residues within approximately 4.0 Å of atoms in the metal cluster are shown for the *E. halophila* protein (*A*) and the *C. vinosum* molecule (*B*). Note that while Phe-66 (*C. vinosum*) and Phe-53 (*E. halophila*) are conserved between these two molecules, their side chains adopt quite different conformations.

therefore may, in part, account for the exceptionally low oxidation-reduction potential of the *E. halophila* protein. Also, the *E. halophila* HiPIP has a net protein charge of −10 as contrasted with −3 for the *C. vinosum* protein. Again, this larger net negative charge may contribute to the lower redox potential exhibited by the *E. halophila* HiPIP.

Based on the *C. vinosum* HiPIP structure and the three-dimensional comparisons with low potential bacterial ferredoxins, it was suggested that the extent of hydrogen bonding to the redox center plays a critical role in redox potential modulation (Carter *et al.*, 1974, Adman *et al.*, 1975; Carter, 1977). In the *C. vinosum* HiPIP, there are five potential hydrogen bonds to the iron-sulfur cluster while in the *P. aerogenes* low potential ferredoxin there are eight to each cluster. The differences in the oxidation levels used by the HiPIPs as contrasted with the low potential ferredoxins is now thought to be due to both differences in hydrogen bonding and to exposure of the iron-sulfur clusters to the solvent. The more hydrophobic environment of the [4Fe-4S] cluster in the HiPIP with fewer hydrogen bonds favors the −1 oxidation level (Backes *et al.*, 1991).

Perhaps the most striking aspect of the *E. halophila* HiPIP structure is that its hydrogen bonding pattern to sulfurs in the redox center is nearly identical to that observed in the *C. vinosum* HiPIP. As in the *C. vinosum* molecule, there are four potential hydrogen bonds with linear geometry to the cysteine ligands and they are as follows: the sulfur atom of Cys-34 is 3.2 and 3.7 Å from the amide nitrogens of Phe-36 and Ala-68, respectively, the sulfur atom of Cys-48 is 4.0 Å from the amide nitrogen of His-50 and the sulfur atom of Cys-64 is 3.4 Å from the amide nitrogen of Val-66. Likewise, there is a possible hydrogen bond between one of the inorganic sulfurs of the cluster and the amide hydrogen of Cys-64 although the geometry for this interaction deviates significantly from linearity as is also observed in the *C. vinosum* HiPIP. It is noteworthy that the amino acid sequence alignments of Tedro *et al.* (1985), based on primary structure, also predicted that the *E. halophila* HiPIP would have the same hydrogen bonding pattern as that observed in the *C. vinosum* protein.

From the structure determination of the *E. halophila* protein described here it is now apparent that the redox potential difference of 240 mV exhibited by the *E. halophila* and the *C. vinosum* HiPIPs cannot be simply attributed to differences in cluster hydrogen bonding patterns alone. Clearly there are many subtle factors affecting the oxidation-reduction potentials of the iron-sulfur proteins such as peptide chain flexibility, solvent structure, exposure of the [4Fe-4S] to the solvent, the number and positions of hydrophobic amino acid residues surrounding the cluster, and the electrostatic field of the protein. These issues will be addressed in greater depth once the *E. halophila* molecule has been solved and refined to as high a resolution as possible. X-ray coordinates for the *E. halophila* protein have been deposited in the Brookhaven Protein Data Bank or may be obtained immediately via HOLDEN@VMS.MACC·WISC·EDU (INTERNET) or HOLDEN@WISCMACC (BITNET).

Acknowledgment—We would like to thank the reviewer for the very helpful comments and criticisms.

REFERENCES

Adman, E., Watenpaugh, K. D., and Jensen, L. H. (1975) *Proc. Natl. Acad. Sci. U. S. A.* **72,** 4854–4858

Backes, G., Mino, Y., Loehr, T. M., Meyer, T. E., Cusanovich, M. A., Sweeney, W. V., Adman, E. T., and Sanders-Loehr, J. (1991) *J. Am. Chem. Soc.* **113,** 2055–2064

Bartsch, R. G. (1978) *Methods Enzymol.* **53,** 329–340

Bernstein, F. C., Koetzle, T. F., Williams, G. J. B., Meyer, E. F., Jr., Brice, M. D., Rogers, J. R., Kennard, O., Shimanouchi, T., and Tasumi, M. (1977) *J. Mol. Biol.* **112,** 535–542

Blum, M., Metcalf, P., Harrison, S. C., and Wiley, D. C. (1987) *J. Appl. Crystallogr.* **20,** 235–242

Bricogne, G. (1976) *Acta Crystallogr.* **A32,** 832–847

Carter, C. W., Jr. (1977) *J. Biol. Chem.* **252,** 7802–7811

Carter, C. W., Jr., Kraut, J., Freer, S. T., Alden, R. A., Sieker, L. C.,

Adman, E., and Jensen, L. H. (1972) *Proc. Natl. Acad. Sci. U. S. A.* **69,** 3526–3529
Carter, C. W., Jr., Kraut, J., Freer, S. T., Xuong, N.-H., Alden, R. A., and Bartsch, R. G. (1974) *J. Biol. Chem.* **249,** 4212–4225
Chu, C. T-W., Lo, F., Y-K., and Dahl, L. F. (1982) *J. Am. Chem. Soc.* **104,** 3409–3422
Dus, K., Tedro, S., Bartsch, R. G., and Kamen, M. D. (1971) *Biochem. Biophys. Res. Commun.* **43,** 1239–1245
Freer, S. T., Alden, R. A., Carter, C. W., Jr., and Kraut, J. (1975) *J. Biol. Chem.* **250,** 46–54
Holden, H. M., Meyer, T. E., Cusanovich, M. A., and Rayment, I. (1986a) *J. Biol. Chem.* **261,** 4219–4220
Holden, H. M., Meyer, T. E., Cusanovich, M. A., and Rayment, I. (1986b) *J. Biol. Chem.* **261,** 14746–14747
Holden, H. M., Kanost, M. R., Law, J. H., Rayment, I., and Wells, M. A. (1988) *J. Biol. Chem.* **263,** 3960–3962
Jones, T. A. (1985) *Methods Enzymol.* **115,** 157–171
Meyer, T. E. (1985) *Biochim. Biophys. Acta* **806,** 175–183
Meyer, T. E., Przysiecki, C. T., Watkins, J. A., Bhattacharyya, A., Simondsen, R. P., Cusanovich, M. A., and Tollin, G. (1983) *Proc. Natl. Acad. Sci. U. S. A.* **80,** 6740–6744
Rayment, I. (1983) *Acta Crystallogr.* **A39,** 102–116
Rossmann, M. G. (1960) *Acta Crystallogr.* **13,** 221–226
Rossmann, M. G., and Argos, P. (1975) *J. Biol. Chem.* **250,** 7525–7532
Rypniewski, W. R., Breiter, D. R., Benning, M. M., Wesenberg, G., Oh, B-H., Markley, J. L., Rayment, I., and Holden, H. M. (1991) *Biochemistry* **30,** 4126–4131
Sheridan, R. P., Allen, L. C., and Carter, C. W., Jr. (1981) *J. Biol. Chem.* **256,** 5052–5057
Spiro, T. G. (1982) in *Iron-Sulfur Proteins,* John Wiley & Sons, New York
Strombaugh, N. A., Sundquist, J. E., Burris, R. H., and Orme-Johnson, W. H. (1976) *Biochemistry* **15,** 2633–2641
Tedro, S. M., Meyer, T. E., and Kamen, M. D. (1985) *Arch. Biochem. Biophys.* **241,** 656–664
Terwilliger, T. C., and Eisenberg, D. (1983) *Acta Crystallogr.* **A39,** 813–817
Thaller, C., Weaver, L. H., Eichele, G., Wilson, E., Karlsson, R., and Jansonius, J. N. (1981) *J. Mol. Biol.* **147,** 465–469
Thaller, C., Eichele, G., Weaver, L. H., Wilson, E., Karlsson, R., and Jansonius, J. N. (1985) *Methods Enzymol.* **114,** 132–135
Thomson, A. J. (1985) in *Metalloproteins Part I* (Harrison, P., ed) pp. 79–120, Verlag Chemie, Deerfield Beach, FL
Tronrud, D. E., Ten Eyck, L. F., and Matthews, B. W. (1987) *Acta Crystallogr.* **A43,** 489–501